AIP | Physics of Fluids

Turbulence in vertical axis wind turbine canopies

Matthias Kinzel, Daniel B. Araya, and John O. Dabiri

Citation: Physics of Fluids **27**, 115102 (2015); doi: 10.1063/1.4935111
View online: http://dx.doi.org/10.1063/1.4935111
View Table of Contents: http://scitation.aip.org/content/aip/journal/pof2/27/11?ver=pdfcov
Published by the AIP Publishing

PHYSICS OF FLUIDS **27**, 115102 (2015)

Turbulence in vertical axis wind turbine canopies

Matthias Kinzel,[1] Daniel B. Araya,[1] and John O. Dabiri[1,2,a)]
[1]*Graduate Aerospace Laboratories, California Institute of Technology, Pasadena, California 91125, USA*
[2]*Bioengineering, California Institute of Technology, Pasadena, California 91125, USA*

(Received 10 February 2015; accepted 20 October 2015; published online 9 November 2015)

Experimental results from three different full scale arrays of vertical-axis wind turbines (VAWTs) under natural wind conditions are presented. The wind velocities throughout the turbine arrays are measured using a portable meteorological tower with seven, vertically staggered, three-component ultrasonic anemometers. The power output of each turbine is recorded simultaneously. The comparison between the horizontal and vertical energy transport for the different turbine array sizes shows the importance of vertical transport for large array configurations. Quadrant-hole analysis is employed to gain a better understanding of the vertical energy transport at the top of the VAWT arrays. The results show a striking similarity between the flows in the VAWT arrays and the adjustment region of canopies. Namely, an increase in ejections and sweeps and decrease in inward and outward interactions occur inside the turbine array. Ejections are the strongest contributor, which is in agreement with the literature on evolving and sparse canopy flows. The influence of the turbine array size on the power output of the downstream turbines is examined by comparing a streamwise row of four single turbines with square arrays of nine turbine pairs. The results suggest that a new boundary layer forms on top of the larger turbine arrays as the flow adjusts to the new roughness length. This increases the turbulent energy transport over the whole planform area of the turbine array. By contrast, for the four single turbines, the vertical energy transport due to turbulent fluctuations is only increased in the near wake of the turbines. These findings add to the knowledge of energy transport in turbine arrays and therefore the optimization of the turbine spacing in wind farms. [http://dx.doi.org/10.1063/1.4935111]

I. INTRODUCTION

A. Energy production in large wind turbine arrays

With wind farms increasing in size, the focus in research is shifting from the efficiency of single wind turbines to the overall performance of the turbine array (see, e.g., Refs. 1 and 2). The work can be divided into two categories: wind turbine wakes, wake interaction and influence on the downwind turbines (e.g., Refs. 3, 5, and 6) and the energy transfer between the turbine array and the surrounding atmospheric surface layer flow (see Refs. 7–10).

Due to the large dimensions of both the turbine arrays as well as the turbines themselves, few experiments have been done in the field (e.g., Refs. 5, 11, and 12), whereas most of the above mentioned studies were conducted in wind tunnel experiments and numerically. The laboratory experiments have the limitation that it is challenging to match the high Reynolds number and the turbine blade tip speed ratio simultaneously in a wind tunnel without motorizing the wind turbines. The high Reynolds number of the flow and the wind farm dimensions on the order of kilometers also limit the numerical work to mainly wall modeled large eddy simulations (LES) (see, e.g., Ref. 10).

a)Electronic address: jodabiri@stanford.edu. Current address: School of Engineering, Stanford University, Stanford, California 94305, USA.

The velocity in the wake of a horizontal axis wind turbine (HAWT) takes on the order of 20 rotor diameters to recover to the upstream value (see, e.g., Ref. 13). Therefore, a typical turbine spacing of 10 rotor diameters decreases the power output of the downstream turbine by as much as 40% (see Ref. 14). Meyers and Meneveau[2] recommended an optimal turbine spacing of 16-18 rotor diameters from an economical point of view.

Some studies have investigated algorithms that limit the power output of individual turbines in order to optimize the overall power output and grid performance by the turbine array (see, e.g., Refs. 15–17). Most studies, however, analyze the energy transport within the turbine array with the aim to optimize the turbine spacing. In this context, Cal *et al.*[7] derived equations for the kinetic energy transport from the Reynolds-averaged Navier-Stokes equation for the streamwise direction,

$$\langle\overline{u}\rangle\frac{\partial\frac{1}{2}\langle\overline{u}\rangle^2}{\partial x}+\langle\overline{w}\rangle\frac{\partial\frac{1}{2}\langle\overline{u}\rangle^2}{\partial z}=-\frac{1}{\rho}\langle\overline{u}\rangle\frac{dp_\infty}{dx}-\frac{\partial}{\partial z}\left(\left\langle\overline{u'w'}\right\rangle\langle\overline{u}\rangle+\left\langle\overline{u''w''}\right\rangle\langle\overline{u}\rangle\right)+\left\langle\overline{u'w'}\right\rangle\frac{\partial\langle\overline{u}\rangle}{\partial z}+\left\langle\overline{u''w''}\right\rangle\frac{\partial\langle\overline{u}\rangle}{\partial z}-P(z). \tag{1}$$

In the equation above, primes indicate turbulent fluctuations, over bars temporal averaging, and angle brackets spatial averaging in the horizontal plane. u and w are the streamwise and vertical velocities along the x and z directions. The dispersive stress, $\left\langle\overline{u''w''}\right\rangle$, is caused by the correlation between spatially non-homegeneous horizontal and vertical mean velocities. It is defined as $\overline{u}''=\overline{u}-\langle\overline{u}\rangle$ and $\overline{w}''=\overline{w}-\langle\overline{w}\rangle$. Cal *et al.*[7] show that this term is small compared to the Reynolds stresses, $\left\langle\overline{u'w'}\right\rangle$, which is why it will not be considered in the following analysis of the planform momentum flux. $P(z)$ results from the product of the spatially averaged velocity, $\langle\overline{u}\rangle$, and the averaged thrust force, $\left\langle\overline{f_x}\right\rangle$. The viscous terms are neglected because of the high Reynolds number of the flow ($Re\approx10^6$). The Coriolis force term can also be neglected due to the Rossby number being $Ro=\frac{U}{fL}\gg1$, where $U\approx10$ m s^{-1} is the characteristic velocity, $f=2\Omega sin\varphi\approx10^{-4}$ rad/s is the Coriolis frequency, and $L=40$ m the maximum characteristic length scale of the turbine arrays.

From the kinetic energy equation (Equation (1)), it can be seen that there are two ways that energy enters a turbine array: horizontally from the sides and vertically from above. The corresponding terms are

$$\left\langle\overline{P}_s\right\rangle=\frac{1}{2}\rho A_s\langle\overline{u}\rangle^3 \tag{2}$$

for the streamwise transport by the mean flow and

$$\left\langle\overline{P}_p\right\rangle=-\rho A_p\langle\overline{u}\rangle\left\langle\overline{u'w'}\right\rangle \tag{3}$$

for the vertical energy transport by the turbulent stresses as well as

$$\left\langle\overline{P}_t\right\rangle=\frac{1}{2}\rho A_t\langle\overline{u}\rangle^3, \tag{4}$$

for the transverse energy transport. A_s, A_p, and A_t denote the projected area of the turbine array in the streamwise, planform, and transverse direction, respectively. The planform energy transport, P_p, is defined negative such that positive values correspond to a momentum flux into the turbine array.

Once the energy from the horizontal flux has been converted into power by the turbines in the upstream rows or dissipated by viscous stresses the planform momentum flux becomes the main source of energy (see, e.g., Ref. 7). Therefore, the vertical energy transport becomes more important with increasing size of the turbine array. This necessitates a compromise because while the vertical momentum flux increases with the turbulence levels above the wind farm, a higher turbulence intensity inside the wind farm increases the stress on the turbine structures.

Recent studies by Whittlesey *et al.*[18] and Dabiri[19] suggest that vertical-axis wind turbines (VAWTs) can be spaced more closely than HAWTs without a decrease in the power output of the individual turbines. As a result, VAWT wind farms might be able to achieve a higher energy output per footprint area than HAWT farms. In an effort to understand the different wake recovery between

VAWT and HAWT turbine arrays, Kinzel *et al.*[12] examined the wakes of VAWTs in a small array setting as well as the vertical energy transport. The present study analyzes the flow phenomena that lead to the vertical energy transport.

B. Canopy flows and quadrant-hole (Q-H) analysis

Due to the potentially close spacing of the turbines in VAWT arrays, the vertical energy transport shares similarities with canopy flows. Canopy flows are of interest in the context of urban and agricultural applications and also in atmospheric science (see, e.g., Refs. 20 and 21).

The VAWT array investigated presently is not sufficiently large to form a fully developed canopy flow. Therefore, our focus is on the *adjustment region* between the atmospheric surface layer and the canopy. As described in the work of Belcher *et al.*,[22] the drag of the canopy elements decelerates the air which increases the mean pressure. This pressure gradient extends into an *impact region* upstream of the canopy where it decreases the flow velocity. The flow velocity is further decreased in the *adjustment region* behind the leading edge of the canopy. The deceleration of the flow in this region causes a vertical flux out of the center of the canopy as required by conservation of mass. Simultaneously, energy is transported into the canopy by the turbulence stresses, $\langle\overline{u'w'}\rangle$. At the end of the *adjustment region*, the downward momentum transport and the power required to overcome the aerodynamic drag of the canopy elements reach a local balance.

In order to analyze the vertical momentum transport, the Reynolds stress tensor, $\langle\overline{u'w'}\rangle$, can be decomposed into four quadrants (see, Ref. 23). A sketch of these four quadrants can be found in Figure 1. The first quadrant represents outward interactions ($u' > 0, w' > 0$) which corresponds to high momentum fluid exiting the canopy. The second quadrant represents low momentum fluid being ejected from the canopy ($u' < 0, w' > 0$). Low momentum fluid entering the canopy ($u' < 0, w' < 0$), called inward interactions are captured by the third quadrant. Finally, the fourth quadrant represents sweeps of high momentum fluid entering the canopy ($u' > 0, w' < 0$).

As mentioned by Belcher *et al.*,[22] ejections are dominant in the canopy *adjustment region*. This dominance is also reported for sparse canopies by Katul *et al.*[21] Yue *et al.*[24] report that sweeps are the largest contributor to the downward turbulent energy transport inside the developed canopy area. Inward and outward interactions are reported to be smaller in magnitude than sweeps and ejections. This is consistent with turbulence causing a net momentum transport into the canopy.

In Q-H analysis (see, e.g., Refs. 23 and 24), a hyperbolic curve is defined in the $u' - w'$ plane by the hole size H as

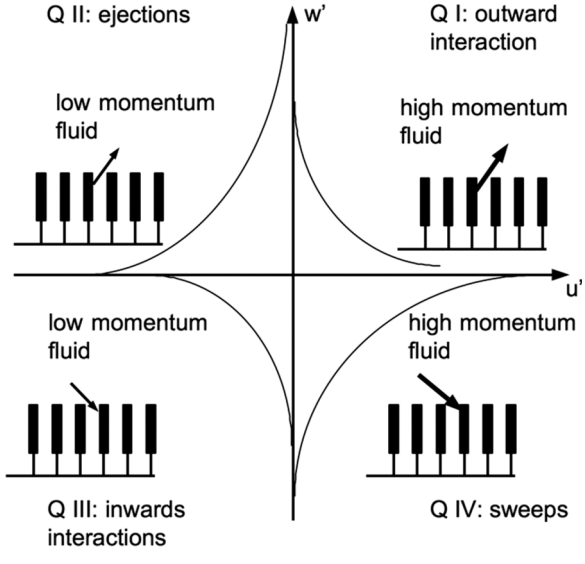

FIG. 1. Schematic of the quadrant-hole plot.

$$H = \frac{|u'w'|}{|\overline{u'w'}|}. \tag{5}$$

The method utilizes a conditional sampling function, I, to determine if a turbulent event falls into a certain quadrant and hole size,

$$I_{i,H,t}(u'w') = \begin{cases} 1 & \text{if } u'w' \text{ lies in quadrant i and } |u'w'| \geq H|\overline{u'w'}| \\ 0 & \text{otherwise} \end{cases}.$$

The conditional sampling function is used to define the mean quadrant events over time, t, such as the Reynolds shear stress, $S_{i,H}$, which is the negative of the momentum flux,

$$S_{i,H} = \frac{1}{T}\int_0^T u'w' I_{i,H,t} dt. \tag{6}$$

The duration of the events is given by

$$D_{i,H} = \frac{1}{T}\int_0^T I_{i,H,t} dt. \tag{7}$$

T stems from the time period of the data. Together, $D_{i,H}$ and $S_{i,H}$ provide information about the amount of momentum flux that is transferred into the canopy by sweeps and ejections and out of the canopy by inwards and outwards interactions. The analysis of these two quantities also shows at which scale this transport is accomplished, e.g., if the majority of energy that is transferred into the canopy by sweeps is due to a large number of small turbulent fluctuations or by a smaller number of large amplitude events (see, e.g., Ref. 24).

II. METHODS

A. Experimental methods

Experiments were conducted at the Caltech Field Laboratory for Optimized Wind Energy (FLOWE) located in the Antelope valley of northern Los Angeles County in California, USA. The surroundings are flat desert terrain for at least 1.5 km in each direction. The desert to the northeast and the ocean to the southwest create high wind velocities with a prevailing wind direction almost year round. The turbines are typically in operation when the atmospheric boundary layer is not neutrally stable. Therefore, buoyancy effects contribute to the turbulence levels of the flow.

This study focuses on arrays of eighteen VAWTs positioned in nine counter-rotating pairs (Figure 2(a)). The turbines within a pair are located 1.65 rotor diameters apart from each other and

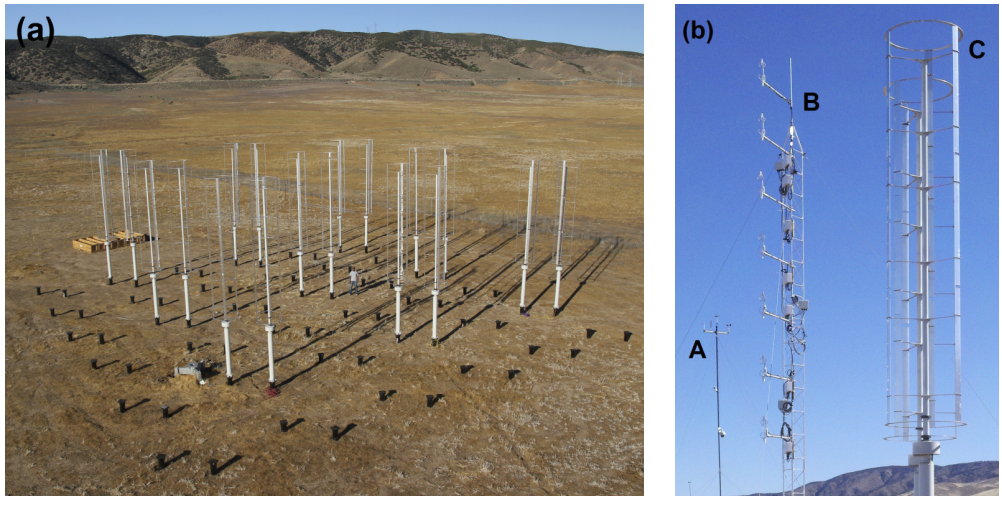

FIG. 2. (a) Image of the 18 turbine array and (b) close up of reference measurement tower (A), the measurement tower with the ultrasonic anemometers (B), and a counter-rotating turbine pair (C).

the pairs are spaced on an 8D by 8D grid. Two different turbine configurations were tested: one where the counter-rotating turbine pair resembles a potential flow doublet (i.e., the airfoil shaped blades move upwind in the area at the center of the turbine pair) and one where they form a reverse doublet. The two cases will be referred to as doublet and reverse doublet configurations in the following. A sketch of these two configurations together with a wind rose summarizing the wind conditions during the time of the measurements can be found in Figure 3(a) and 3(b), respectively. Furthermore, an array of four single turbines with a spacing similar to the turbines along the center-line of the 18 turbine arrays was analyzed for comparison. A sketch of this array and the wind speed and direction is depicted in Figure 3(c).

A close up picture of a turbine pair and the measurement equipment can be seen in Figure 2(b). The turbines are 1.2 kW VAWTs (Windspire Energy, Inc.). They have a total height of 9.1 m, a rotor height of 6.1 m, and a diameter of 1.2 m. Their maximum rotation rate is 420 rpm at a wind speed of 12 m s^{-1}, which corresponds to a tip speed ratio of $\Omega = 2.3$. The cut-in and cut-out speeds for this turbine are 3.8 m s^{-1} and 12 m s^{-1}, respectively.

The wind velocities were measured using a portable 10 m high meteorological tower (Alumna Towers, Inc.) with seven, vertically staggered, three-component ultrasonic anemometers (CSAT3 by Campbell Scientific, Inc.). The sensors are equally spaced at heights between the top and the bottom of the turbine rotor, i.e., between heights of 3 m and 9 m, see Figure 2. The CSAT3 sensors acquired data at a sampling rate of 10 Hz with an accuracy of ± 0.161 m s^{-1}. The velocity profiles were measured at several locations along the center line of the turbine arrays as sketched in Figure 3. For the doublet configuration, these positions were 15D and 1.5D upstream as well as 2D, 8D, 18.5D, 24D, 29D, and 37D downstream from the front of the array; for the reverse doublet configuration, the measurement locations were 2D, 8D, 13D, 19D, 24D, and 30D downwind; and for the single turbine configuration, the locations were 2D upstream as well as 2D, 8D, 13D, 19D, 24D, 30D, 35D, and 41D downstream.

The measurements were taken for at least 150 h at each position. The data set was filtered for times when the free stream velocity was within the cut-in and cut-out speeds of the turbines and the wind direction was within $\pm 10°$ from the array center line. This filter resulted in no data being available for the measurement locations 13D downstream inside the doublet and 2D upstream of the reverse doublet array, respectively. Since the measurements were conducted consecutively, the data from the different measurement locations were conditioned using the wind speed and direction information from a 10 m high reference meteorological tower located to the southeast of the turbine array (compare Figure 3). The anemometer used for the reference measurement (Thies First Class) recorded data at 1 Hz with an accuracy of $\pm 3\%$. The reference meteorological tower can also be seen in the background of Figure 2(b). Ten minute averages of the reference velocity are used to normalize the data from the CSAT3 sensors that were recorded during the corresponding interval. These intervals are filtered to span the operational velocity range of the VAWTs, i.e., the lower and upper bounds coincide with the cut-in and cut-out speeds of the turbines. Furthermore, the information from the reference sensor facilitated conditioning of the data for wind directions of $215 < \alpha < 235$. The full data set is available for download at http://www.flowe.caltech.edu.

The mean horizontal wind speeds as measured by the reference sensor were 8.24 m s^{-1}, 8.14 m s^{-1}, and 8.45 m s^{-1} during the times when the doublet, reverse doublet, and four single turbine configurations were tested leading to an average Reynolds number of $\approx 10^6$ based on rotor diameter. The prevailing wind direction was south-southwest, i.e., 223°, 228°, and 234° for doublet, reverse doublet and four turbine configurations, respectively. This can also be seen in the wind roses depicted on the right side of Figure 3.

For further analysis of the conditions in which the turbines operate, Figure 4(a) presents the horizontal wind speed and the temperature over the time of day. The data are averaged over a period of one week and the standard deviation, which is indicated by the errorbars, is calculated over 10 min intervals. The wind velocity and temperature exhibit their lowest values at approximately 7 am and 6 am, respectively. From there, the temperature rises until approximately 3pm and the wind velocity follows with a time delay. Both quantities decline during the late afternoon and evening hours, plateau during the first half of the night, and then further decrease until they reach

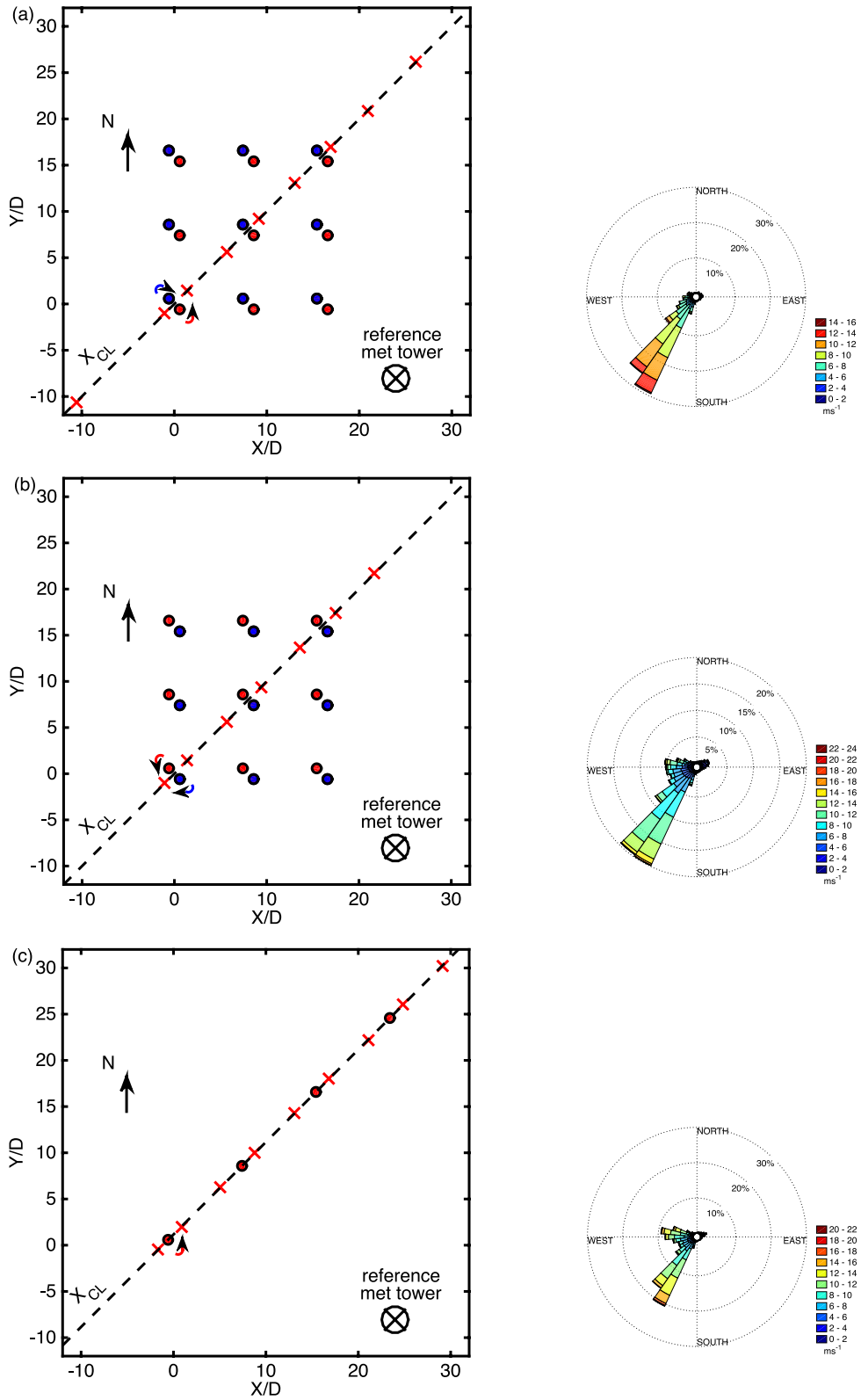

FIG. 3. Sketch of the measurement setup (left) and wind rose for the time of the measurement duration (right) for the doublet (a), reverse doublet (b), and four single turbine (c) configurations. Red circles symbolize counter clockwise rotating turbines, blue circles clockwise rotating turbines, red crosses the measurement locations, and X_{cl} is the coordinate along the measurement transect following the array center line.

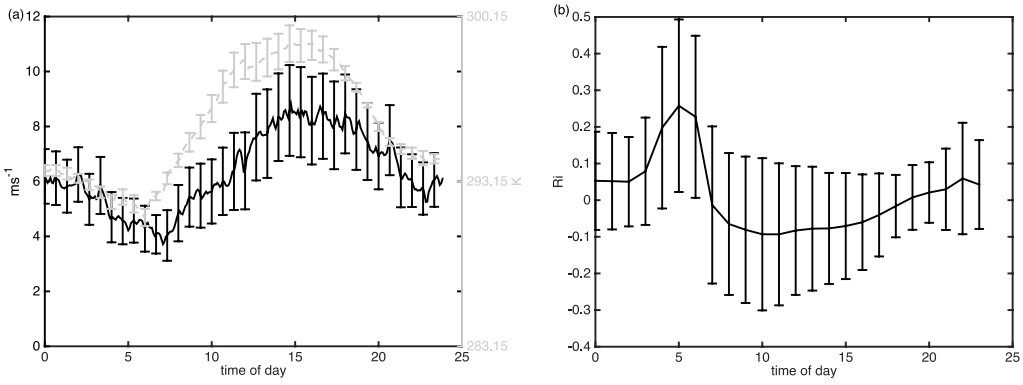

FIG. 4. (a) Horizontal wind velocity (solid) and temperature (dashed) for the time of day. (b) Bulk Richardson number (solid) for the time of day. Errorbars denote one standard deviation.

the before mentioned minimums. The bulk Richardson number is defined as

$$Ri = \frac{g}{\overline{\theta_v}} \frac{\frac{\partial \overline{\theta_v}}{\partial z}}{\left(\frac{\partial \overline{u}}{\partial z}\right)^2 + \left(\frac{\partial \overline{v}}{\partial z}\right)^2}, \tag{8}$$

where g is the gravitational constant, θ_v the potential temperature, and z the vertical direction in which the temperature and velocity gradients are calculated. As described in Ref. 4, Ri signals large levels of turbulence due to wind shear when it is small and negative. The wind forces are also dominant when Ri is small and positive. However, in the latter case, the flow is weakly stable. Jacobson[4] states the critical Richardson number at which a laminar flow becomes turbulent as 0.25 and the termination Richardson number at which turbulent flow turns laminar as 1.0.

Figure 4(b) shows the Richardson number over the time of day. Again the data are averaged over a period of one week. The atmospheric surface layer is weakly stable in the early morning hours with a peak in Ri around 5 o'clock. During the daytime, the flow is turbulent and dominated by shear from the wind velocities. Ri turns negative around the time when the wind velocities start to increase in the morning and turns positive when the velocities start to decrease in the evening. Considering the cut-in wind speed of the turbines, it can be assumed that the turbines are producing most of their power at times when the atmospheric surface layer is unstable.

During all measurement campaigns, the power output of each turbine was monitored using a WattNode Modbus (Continental Control Systems LLC). These sensors have an accuracy of ±0.5% when the measured current is between 5% and 100% of the rated current. The accuracy reduces to ±1%–3% when the WattNode is operated outside of these boundaries. Similarly to the reference wind data, the turbine power was sampled at 1 Hz and stored as 10 min averages. The power coefficient, C_p, is a measure of the wind turbine efficiency, i.e., the turbine power output normalized by the available energy in the flow. This metric is defined as

$$C_p = \frac{P_{turbine}}{\frac{1}{2}\rho A |\mathbf{U}|^3}, \tag{9}$$

where $P_{turbine}$ is the power output of the respective turbine, ρ is the density of the fluid, A is the projected area of the turbine, and $\mathbf{U}$ is the characteristic wind velocity vector containing the three velocity components u_{ref}, v_{ref}, and w_{ref}. The characteristic wind velocity is measured by the reference tower outside of the turbine canopy at a height of 10 m, i.e., one meter above the turbine rotors. Therefore, the calculated C_p is more conservative in comparison to the common procedure for HAWTs where the reference velocity is taken at the center of the rotor. In Sec. III, the energy transfer between the atmospheric surface layer and the turbine canopies is measured by calculating a power coefficient based on the turbine power output and the energy available in the free stream. Therefore, these power coefficients include the turbine efficiency as well as the efficiency of the energy transfer between the atmospheric surface layer and the turbine canopy. For the configuration

of four single VAWTs, the turbines could be calibrated allowing for C_p to capture only the efficiency of the energy transfer.

III. RESULTS

A. Mean velocity and power

Since the power production of the turbines is proportional to the cube of the streamwise wind velocity, the relationship between these two quantities is analyzed first. Figure 5(a) presents the normalized streamwise velocity, $u/\mathbf{U}$, and (b) the average turbine power coefficient, C_p, as measured along the center line of the array for the doublet (red), reverse doublet (green), and four single turbine (blue) configurations. The velocities were measured at locations roughly 2D in front of the turbine arrays as well as 2D and 8D downwind from the turbine pairs along the array center line and at the same distances relative to the single turbines, respectively. Furthermore, there were measurements taken 15D upstream and downstream of the 18 turbine array. The exact locations are listed in Section II.

One observable trend is that the flow velocity decreases to approximately 80% of the free stream velocity as it approaches the turbine array. This is caused by a combination of the blockage effect of the turbines and the fact that the free stream velocity is measured at a height of 10 m above ground while the centerline velocity along the array is derived as an average of the sensors that are equally spaced between 3 m and 10 m above ground. Each of these effects accounts for approximately half of the upstream velocity reduction based on the data that were collected at the location 15D upstream of the array. Within the array, the streamwise velocity decreases further as each turbine extracts energy from the flow. The velocity then increases again in the wake region

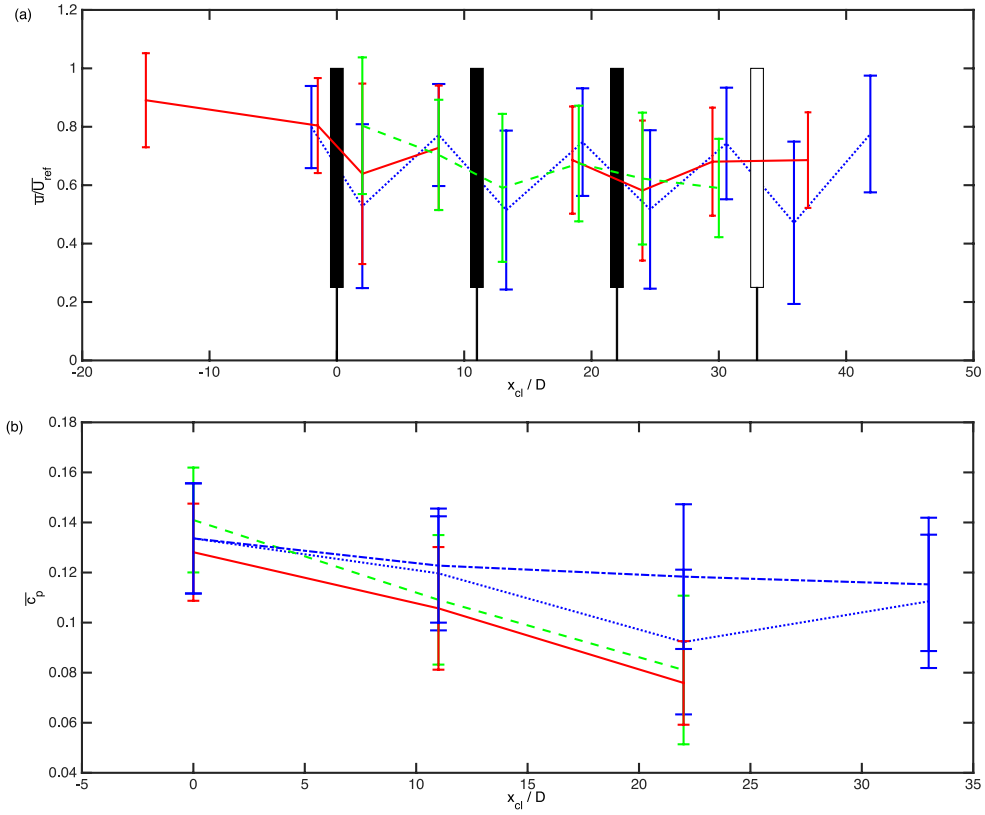

FIG. 5. (a) Normalized velocity and (b) time averaged power coefficient for the doublet (solid), reverse doublet (dashed), and single (dotted) turbine configurations as well as calibrated power coefficients of the four single turbine configuration (dashed-dotted). Black shapes symbolize turbine positions along array centerlines. Error bars denote one standard deviation.

of the individual turbines as well as behind the array. For the turbine pairs, the resulting flow velocities are around 60% of the freestream at 2D and 70% at 8D behind the turbines. The region behind the first turbine pair experiences slightly higher flow velocities as it is more exposed to the freestream flow. Interestingly, the flow only recovers to 70% of the freestream value at the location 15D downstream of the 18 turbine array.

For the four single turbines, the flow velocities drop to approximately 50% and recover to around 75% of the freestream velocity at the positions 2D and 8D behind the turbines, respectively. The lower flow velocity measured immediately behind the single turbines could be attributable to the fact that the measurement location is located behind the turbine instead of between the two turbines that make up a pair. A reason for the higher recovery in the wake behind the single turbines is the lack of blockage that comes from the surrounding turbines in the larger arrays.

C_p is calculated with the freestream velocity $\mathbf{U}$. While this underestimates the efficiency of the downstream turbines, it allows to evaluate the performance of the energy transport inside the array. The energy transport inside the turbine array is the main reason for the changes in C_p since the turbine efficiency varies little between the cut-in and cut-out wind velocities. The average C_p values for each of the four single turbines is calibrated with the turbine C_p measured when the wind was coming from a direction perpendicular to the line of turbines (dashed-dotted line in Figure 5(b)). This was not possible for the turbines along the center line of the 18 turbine arrays due to the obstruction of adjacent turbines. Therefore, the measured C_p of these turbines depend not only on the flow but also on the efficiency of the individual turbines, which exhibited small differences attributed to their manufacturing. The calculated C_p is averaged over the two turbines of a pair in order to lessen this effect. The power production is the lowest for the doublet configuration with C_p values of 0.128, 0.106, and 0.076 for the turbines of the first, second, and third turbine pairs along the array center line. The respective C_p values for the reverse doublet configuration are 0.141, 0.109, and 0.081. While the values of the reverse doublet case are slightly higher than for the doublet case, the slope of the curves is nearly identical, suggesting that the decay in the flow velocities inside the arrays is very similar. The C_p curve for the four single turbines on the other hand decreases less significantly with values of 0.134, 0.123, 0.118, and 0.115. Interestingly, C_p of the turbine in the first row of the four single turbines falls right in between the C_p of the turbines in the first rows of the doublet and reverse doublet configurations. For the doublet configuration, C_p decreases by 17% between the first and the second and by 28% between the second and third turbine rows. The corresponding values for reverse doublet configuration are 23% and 26%. For the four single turbines, C_p decreases 8%, 4%, and 3% between the first, second, and third turbine rows. The decreases in power output are consistent with the decreases in the velocities between the areas in front of the first, second, and third turbine rows considering the $P \propto u^3$ relationship. Since the value of the streamwise velocity is similar behind the second and third turbine pairs, the power production of additional rows located further downstream would most likely not decrease as significantly.

Instead of the turbine power coefficients, the power drop between the most upstream turbines and the corresponding downstream turbines can be calculated in order to analyze the performance of a turbine array. This method has the disadvantage that the values representing the turbines' performance depend not only on the flow and the efficiency of the turbine that is analyzed but also on the efficiency of the most upstream turbine. Mechali *et al.*[5] use this method to investigate the data from the Horns Rev HAWT array off the shore of Denmark. This array consists of an 8 by 10 grid of 2 MW Vestas HAWTs with a rotor diameter of 80 m and a hub height of 70 m. The layout of this array can be seen in Figure 6(a). The spacing of the turbines is 7D in north-south as well as in east-west direction resulting in a spacing of 9.9D along the array diagonal. This is similar to the 8D by 8D spacing of the turbine arrays tested at FLOWE. The spacing of the turbines, which are located in pairs in the transverse direction, is smaller resulting in a higher energy density. Mechali *et al.*[5] evaluated three rows with eight turbines each along the array diagonal ($222° \pm 2°$) for times when the wind velocity was aligned with this direction and between 8 and 9 m s^{-1}. In Figure 6(a), the corresponding turbines are enclosed by a black rectangle and the arrow indicates the wind direction. This case is similar to the flow along the VAWT array center line at FLOWE. The power curves corresponding to this wind direction and velocity are presented in Figure 6(b) for the doublet (solid), reverse doublet (dashed), single turbine (dotted), and the HAWT (dashed-dotted) arrays. In contrast

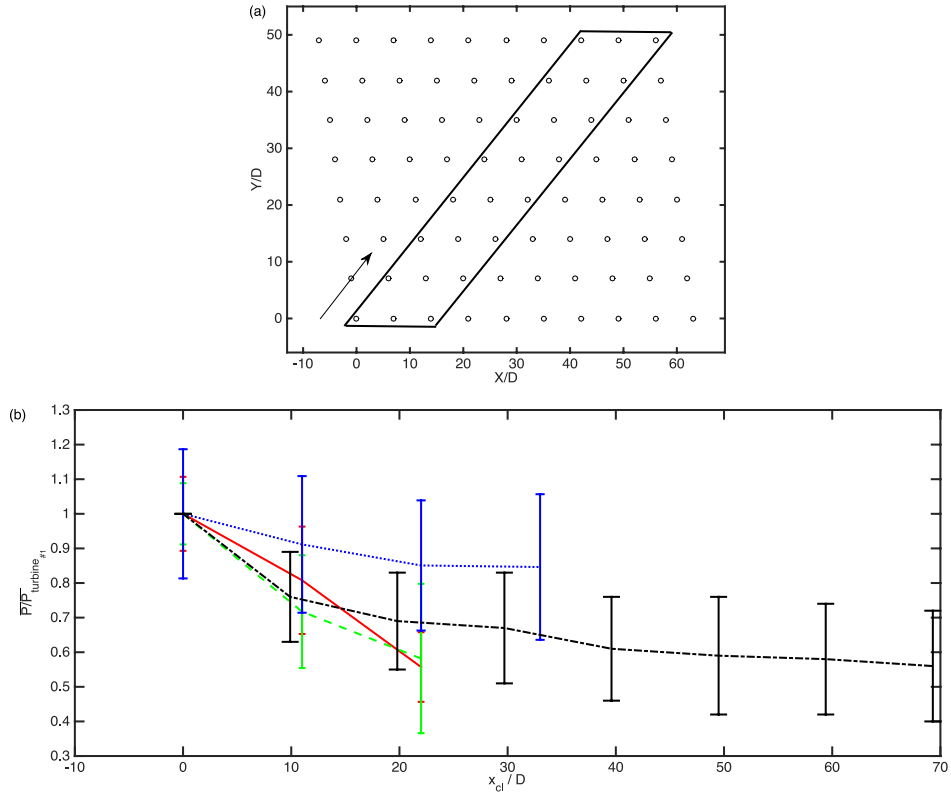

FIG. 6. (a) Sketch of Horns Rev wind farm. The circles symbolize the turbine positions, the arrow the wind direction of $222° \pm 2°$, and the square encloses the three turbine rows for which data was evaluated. (b) Time averaged, normalized power data of the doublet (solid), reverse doublet (dashed), and single (dotted) turbine configurations as well as for the Horns Rev configuration (dashed-dotted) for wind speed between 8 and 9 m s^{-1}. Error bars denote one standard deviation.

to the power coefficient data, these plots show the average power production of the turbines in a given row along the array diagonal normalized with the average power production of the turbines in the most upstream row. As a result, the curves for the power drop look slightly different than the corresponding C_p data. Namely, since the first turbine pair performs better in the reverse doublet than in the doublet configuration, the power drop for the downstream rows is greater for the former even though the C_p of these turbines is higher (compare Figure 5(b)). But in general, it can be observed that the power drop between the 18 turbine VAWT arrays and the turbines along the diagonal of the HAWT array is very similar especially between the first and the second rows. The power drop seems to be slightly higher for the VAWT arrays between the second and third rows. The single turbine configuration performs significantly better than the larger turbine arrays. This suggests that there is a transverse momentum flux even though the mean wind direction is aligned with the turbines and underlines the importance of the vertical energy transport in large turbine arrays. It has to be kept in mind that this direct comparison has its limitations as the two different types of turbines operate at different Reynolds numbers, in different areas of the atmospheric surface layer, and in different terrain. Therefore, the differences in the power output of the downstream turbines do not only result from the differences in the wake structures of HAWTs and VAWTs. Especially, the lower position in the atmospheric surface layer and the larger roughness length of the surrounding terrain cause a higher turbulent mixing rate for the VAWTs. Unfortunately, it is not possible to derive a quantitative estimate for these effects without detailed flow velocity measurements in a HAWT array.

B. Energy transport

The streamwise and planform energy components are analyzed next to gain a better understanding of the kinetic energy that is available inside of the turbine array. For the streamwise energy

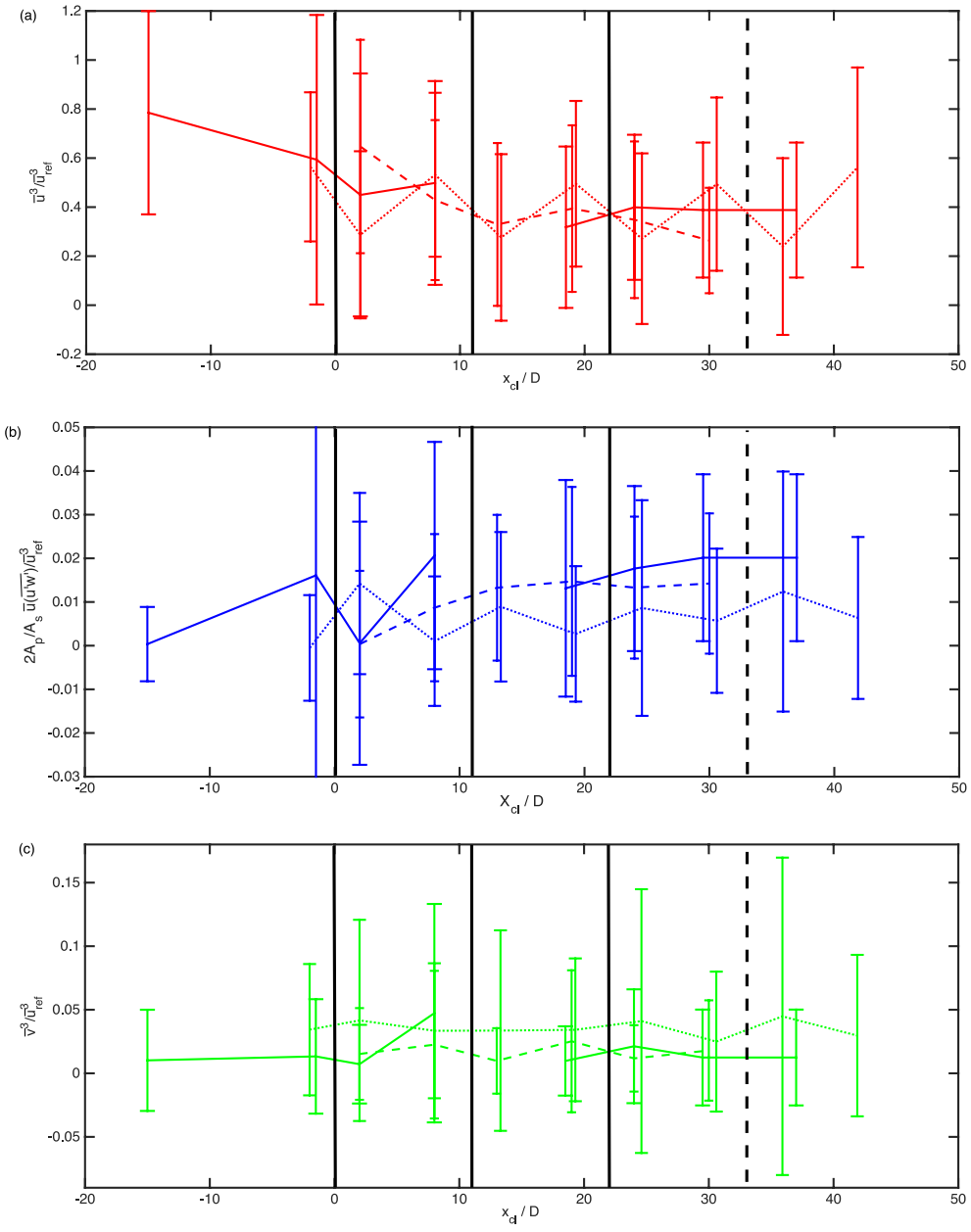

FIG. 7. (a) Streamwise, (b) planform, and (c) transverse normalized power for the doublet (solid), reverse doublet (dashed), and four single turbine (dotted) configurations. Black lines symbolize turbine positions along array centerlines. Error bars denote one standard deviation.

transport, the data are averaged over all seven sensors while only the measurements of the top most sensor is considered for the planform energy component. Figure 7 displays (a) the streamwise, (b) the planform, and (c) transverse energy components normalized with the energy that is available in the free stream, $\overline{P}_s/\overline{P}_{ref} = \overline{u}^3/\overline{u}^3_{ref}$, $\overline{P}_p/\overline{P}_{ref} = 2A_p/A_s\overline{u}\left(\overline{u'w'}\right)/\overline{u}^3_{ref}$, and $\overline{P}_t/\overline{P}_{ref} = \overline{v}^3/\overline{u}^3_{ref}$. Data are presented for the doublet (solid), reverse doublet (dash), and four single turbine (dot) configurations.

The curves for the streamwise energy behave similar to the velocity curves since $P_s \propto u^3$. Namely, this component decreases as the turbines take energy out of the flow and then increases again in the area of the turbine wakes where new energy is brought in through the planform component. There is a clear difference in the behavior of the streamwise energy flux for the 18 turbine

array and the four single turbine configuration. The streamwise energy recovers to more than 90% of the energy in front of the previous turbine in the case of the four single turbines. For the 18 turbine array, it only recovers to about 70% behind the first turbine pair and then starts to recover to about 90% of the value in front of the adjacent upstream turbine pair after that. Furthermore, the streamwise energy does not recover as quickly behind the 18 turbine array as it does behind the last turbine of the four single turbines.

As mentioned before, the energy transferred in the area behind the turbines by the transverse and planform energy components increases the energy contained in the frontal component.

Positive levels of P_p represent energy moving into the array from above. The planform momentum flux is higher in the 18 turbine arrays and also spans a larger area because the turbulence fluctuations at the top of the turbine canopy are higher for the larger arrays. This component is of special importance in large wind farms since it is the only transport mechanism bringing energy to the turbines located in the downwind part of the array after the energy that entered the array from the front and the sides has been depleted. Furthermore, the vertical component of the energy transport depends on the Reynolds stress tensor ($P_p \propto u(u'w')$) and therefore increases with higher turbulence levels. This explains why its levels spike behind the turbines where the turbulence levels are highest. Here as well, there is a difference in the behavior of the energy flux between the 18 and the four single turbine arrays. For the 18 turbine arrays, the planform energy flux increases as the flow approaches the turbine array, declines after the first turbine pair, and then increases to a plateau starting in front of the second turbine pair. For the four single turbine array, the planform energy is the lowest in front of and highest behind the first turbine. Afterwards it is low in front of, and high behind, the consecutive turbines. However, it does not reach the high levels that are exhibited behind the first turbine and also remains lower than the plateaus seen within the 18 turbine arrays. While the measurements show that energy is on average entering the turbine array in the vertical direction, the standard deviation of the planform energy transport is large. This is caused by the turbulence intensity of the flow and suggests that the energy transport is dominated by intense flow events moving fluid with high or low energy into or out of the turbine array. The flow phenomena involved in the vertical energy transport are analyzed and quantified in Sec. III C.

Due to their omni-directionality, VAWTs can also utilize the energy from the transverse momentum flux. However, this is only meaningful in arrays that are small in the transverse direction. The transverse sizes of the arrays under investigation are relatively small, i.e., two orders of magnitude smaller than the atmospheric boundary layer. Nevertheless the momentum flux in the transverse direction is on the same order as the in the planform, see Figure 7(c). The influence of the transverse array size becomes apparent when comparing the data for the four single turbines with that of the two larger arrays. Namely, the transverse momentum flux is approximately twice as large in the four single turbine configuration. The measurements suggest that the power density of the arrays in which the turbines are located in pairs is higher compared to the single turbine configurations over a wide range of inflow angles. For further details about the influence of the inflow angle on the power production of a VAWT pair see Ref. 19.

C. Quadrant-hole analysis

Because of its importance to the energy transport in large wind farms, the planform energy transport is further studied here. Figure 8 presents the results from the quadrant-hole analysis for the (top) doublet, (middle) reverse doublet, and (bottom) four single turbine configurations. The duration of sweeps, ejections, and inward and outward interactions, $D_{i,H}$, is given on the left while the magnitude of the normalized Reynolds stresses of these events, $S_{i,H}$, can be found on the right hand side. The solid lines represent the data from the measurement location 15D upstream of the turbine arrays. The dotted line presents the data from a location 2D and the dashed line from a location 8D (7.5D for the doublet configuration) downwind of a turbine pair. The data 2D downwind of a turbine pair was measured at $X_{cl}/D = 24$, i.e., behind the third turbine row and the data 8D downwind of a turbine pair was taken behind the second turbine row, i.e., at $X_{cl}/D = 19$ ($X_{cl}/D = 18.5$ for the doublet configuration). Data were used from the area behind different turbine rows because of the lack of data immediately behind the second turbine row for the doublet configuration.

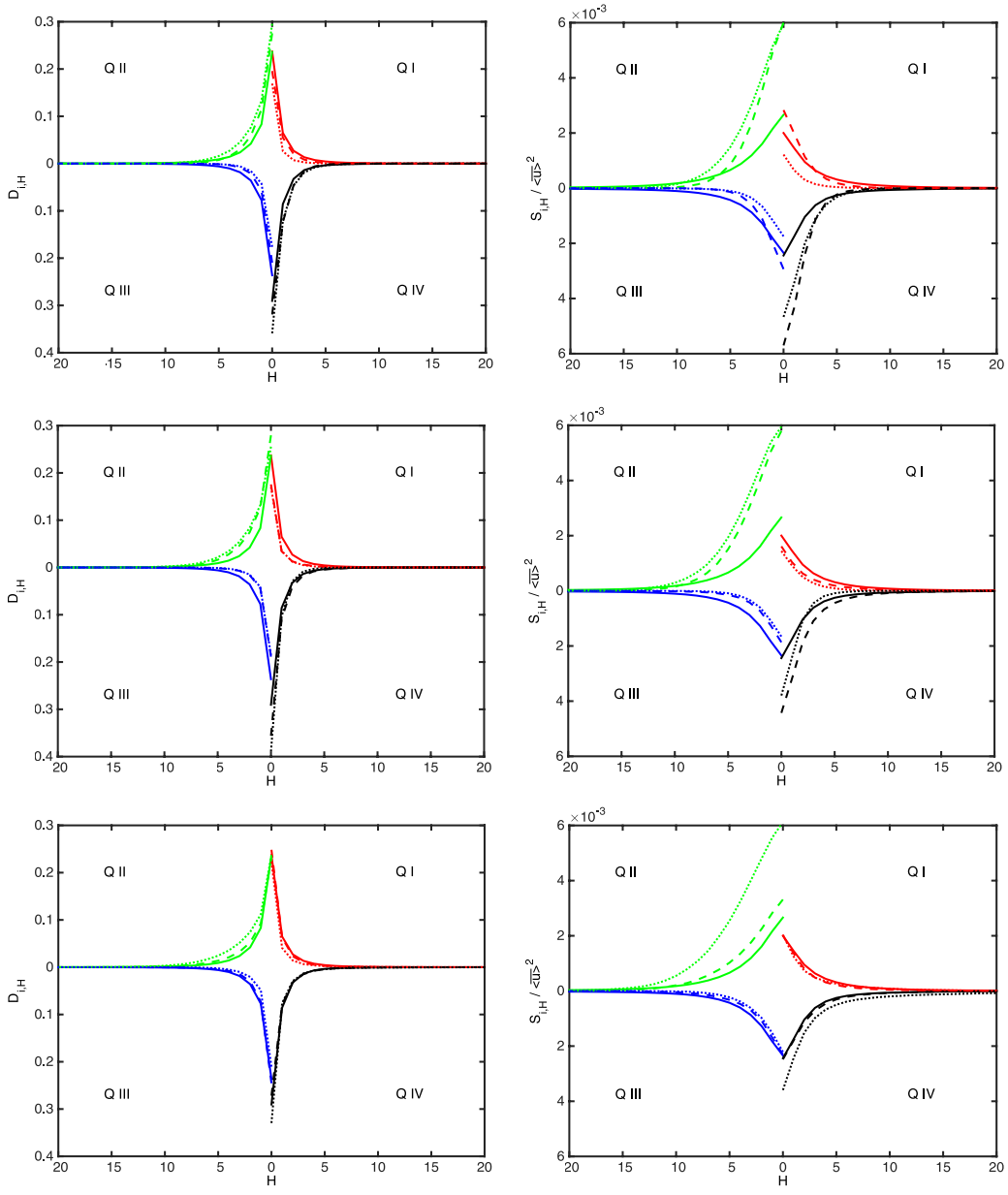

FIG. 8. (Left) Duration and (right) stress of sweeps (black, Q_4), ejections (green, Q_2), inward (red, Q_1), and outward interactions (blue, Q_3) for (top) doublet, (middle) reverse doublet, and (bottom) single turbines configurations. Data are presented for the measurement locations along the array centerlines which are located 15 D upstream (solid) of the array as well as 2D (dotted) and 8D (dashed) downstream of the turbine pairs. (The presented data were measured 2D behind the 3*rd* and 8D behind the 2*nd* turbine rows).

The duration of events appears to be very similar not only between the different turbine configurations but also between the different measurement locations in front of and within the turbine arrays. However, a slight increase in the duration of ejections and sweeps and decrease in inward and outward interactions can be seen between the upstream and the positions within the arrays. More significant, however, is the change in the occurrence of Reynolds stress events both between the different turbine configurations and even more so between the locations within each turbine array.

At the location upstream of the turbine arrays, all four sectors contribute approximately equally to the Reynolds stress tensor. Only ejections occur slightly more often, which is in agreement with

the findings of Belcher *et al.*[22] Within the turbine arrays, however, the occurrence of ejections and, to a slightly lower extent, sweeps increases. Belcher *et al.*[22] also report an increase in ejections in the transition region from an atmospheric surface layer to a canopy flow.

The highest increase can be seen in the ejections measured at the location 2D behind the turbines. The values are similar between the different configurations with the highest levels recorded for the four single turbines followed by the reverse doublet and then the doublet configurations. While the occurrence of ejections remains almost constant between the 2D and 8D locations in the larger arrays, it decreases almost to the level measured upstream of the arrays for the four single turbine configuration.

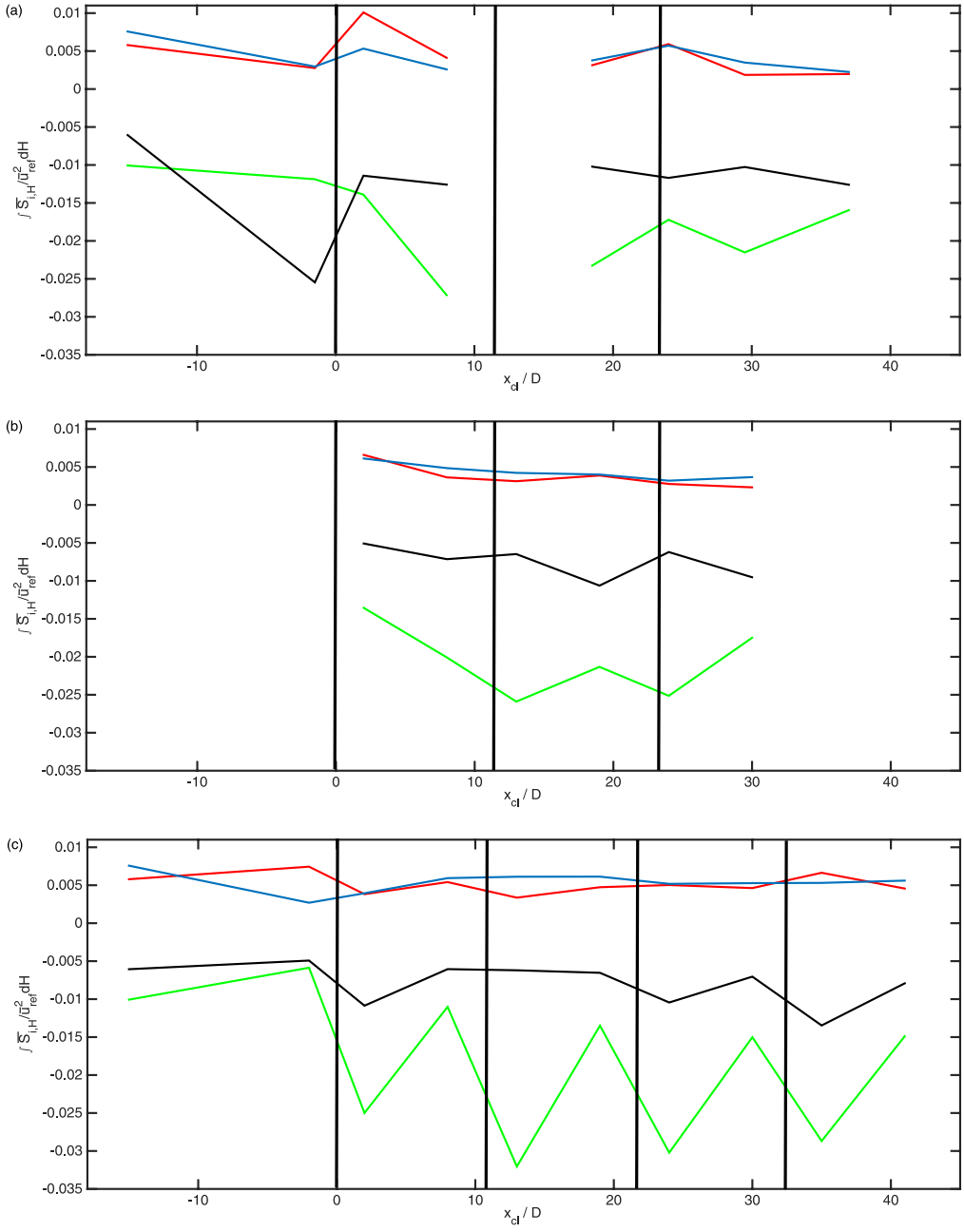

FIG. 9. $\int S_{i,H}\langle\overline{u}_{ref}\rangle^2 dH$ for (a) the doublet, (b) reverse doublet, and (c) the single turbine configurations where (red) lines represent outward interactions, (blue) inward interactions, (green) ejections, and (black) sweeps. Black lines symbolize turbine positions along array centerlines.

Sweeps also exhibit a higher occurrence at the location 2D behind the turbines. While the levels are again very similar between the different configurations at this measurement position, this is not the case further downstream. For the larger arrays, the occurrence of sweep events is even higher at 8D downstream from the turbine pairs than at 2D, while it is almost identical to the upstream values for the four single turbine configuration.

The observation that the occurrence of ejections and sweeps remains elevated within the 18 turbine arrays, whereas it goes down to almost the upstream levels for the four single turbine configuration is in agreement with earlier observations about the behavior of P_p (compare Figure 7(b)).

The impact on inward and outward interactions is not as pronounced. The occurrence of both decreases inside the turbine arrays in comparison to the location 15D upstream. Only for the doublet configuration at the locations 8D behind the turbines and for low H events do they increase.

The plots from the quadrant-hole analysis in Figure 8 represent the flow phenomena at a single measurement location. To achieve a quantitative understanding of the effect of sweeps, ejections, and outward and inward interactions over the whole area of each turbine array, the conditioned Reynolds shear stress of each quadrant was integrated over H. Thus, $\int \overline{S}_{i,H}/\overline{u}^2_{ref} dH$ represents the normalized amount that ejections, sweeps, and inward and outward interactions contribute to the energy transport at the analyzed measurement location. Figure 9 presents the corresponding curves for (a) the doublet, (b) the reverse doublet, and (c) the four single turbine configurations. Outward interactions (red) and inward interactions (blue) are positive as they are transporting energy upwards while ejections (green) and sweeps (black) are negative, transporting energy downwards into the turbine canopy.

For all turbine arrays, the amount of energy that is transported downwards is higher than the amount that is leaving the array at the top. Additionally, ejections are the highest contributor to the planform energy transport followed by sweeps in all cases.

These plots indicate that for the 18 turbine arrays, the amount of energy transported by ejections and sweeps increases and reaches a plateau behind the second turbine pair. The contribution of inward and outward interactions on the other hand decreases and also reaches a plateau behind the second turbine pair. Exceptions are spikes in inward and outward interactions as well as the sweeps around the first turbine pair in the doublet configuration. A possible explanation for this increase in the Reynolds stresses is the exposed position of these first turbine pairs in front of the arrays.

For the four single turbine configuration, inward and outward interactions remain nearly constant throughout the turbine array. Ejections and sweeps do not exhibit the same kind of plateau region that is visible for the larger turbine arrays. Instead, both experience spikes behind the turbines but then fall down to a lower level with downstream distance. The magnitude of the spikes is slightly higher than that of the plateau regions in the 18 turbine arrays.

IV. CONCLUSIONS

Measurements of the streamwise velocity show that the blockage effect of all three turbine arrays is similar at approximately 10%. While this is not surprising when looking at the two 18 turbine arrays, it is noteworthy that an array with three turbine pairs in the transverse direction creates the same effective blockage in the streamwise direction as four single turbines in a row. Within the turbine arrays, the streamwise velocity suggests how the turbines extract energy from the flow and how the energy is replenished in the wake region behind the turbine. As would be expected, the flow recovers more rapidly behind the turbines in the four single turbine configuration. This is especially apparent in the region behind the turbine arrays where the flow recovers to only 70% of the reference streamwise velocity at the measurement location 15D downwind of the 18 turbine array while it recovers to 80% at the location 8D behind the four single turbine configuration.

The trend in the power coefficients of the turbines are in agreement with the data from the streamwise velocity measurements. While C_p decreases form the first to the second and the second to the third turbine pair in the 18 turbine arrays, it remains nearly constant between the turbines in the four single turbine configuration. However, the velocity measurements behind the third turbine pair suggest that the power output of consecutive pairs would be close to that of the third pair. It

appears that the turbines in the reverse doublet configuration perform slightly better than those in the doublet configuration with C_p of the turbine pair in the first row being close to that of the single turbine configuration. However, due to the uncertainties associated with field measurements and the small difference between the performance of the two 18 turbine configurations, this is speculative pending further study.

The comparison between the normalized power data from the three VAWT arrays and HAWT data from Horns Rev suggests that within large arrays, the power drop between downstream turbines is similar between the two turbine types. However, placing the VAWTs in pairs increases the power density of the turbine array compared to HAWTs. This observation is interesting since the wake analysis of isolated vertical axis and horizontal axis turbines suggests that the flow recovers faster behind VAWTs. This faster recovery can be seen in the four single turbine configuration. Further study is needed because while both types of turbine arrays were spaced similarly in the downstream direction in terms of rotor diameter, the respective turbines were operated at different Reynolds numbers and in different parts of the atmospheric surface layer.

Evaluating the streamwise and planform components of the momentum flux highlights the importance of the planform energy transport for large wind farms. While the streamwise energy transport is dominant in the upstream rows of the array, the planform component brings new energy for the downstream turbines. This is especially important since the transverse component seems to decrease quickly with the turbine array size in this direction. The planform component is higher for the 18 turbine arrays than for the four single turbine configuration. This is most likely due to the higher turbulence levels at the top of the larger turbine canopy and will therefore only increase with the turbine array size until the flow along the center line has fully adjusted to the new roughness length that is caused by the turbines.

The planform momentum flux was analyzed further using quadrant-hole analysis. The results suggest that there is an analogy between the flow in a dense VAWT array and a plant or urban canopy. That is, they show an increase in ejections and sweeps as well as a decrease in inward and outward interaction events. A key finding is the difference in the occurrence of these flow phenomena between the 18 turbine arrays and the four single turbine configuration. For the larger arrays, ejections and sweeps are increased and inward and outward interactions decreased both at the measurement locations 2D and 8D behind the turbines. However, in the four single turbine array, this increase and decrease in the quadrant events is only pronounced at the measurement location close to the turbines and mainly involves an increase in ejections. This suggests again that a new surface layer flow evolves on top of the 18 turbine array while the flow between the four single turbines recovers close to the surface layer flow found upstream of the turbines. This difference between the turbine configurations is further highlighted by looking at the product of the occurrence and the Reynolds stress terms, $S_{i,H}D_{i,H}$, over the whole length of the array centerlines. For the 18 turbine arrays, the magnitude of these flow events changes in the first two turbine rows and then plateaus. For the four single turbine configuration, the magnitude of these flow events keeps increasing and decreasing depending on whether the measurement location is close to or further away from a turbine. These results also underline the finding that ejections are the strongest mechanism for the energy transport in the transition area of the turbine canopy, followed by sweeps and that inward and outward interactions occur less often in comparison to the upstream flow.

These findings show a strong similarity between the flow in VAWT arrays and the adjustment region of canopies. They suggest that a dense spacing of VAWTs can lead to an increase in the planform energy flux over the whole planform area of the turbine array. However, further research is necessary to derive quantitative models for the prediction of the planform energy transport in VAWT arrays based on the current models for canopy flows.

ACKNOWLEDGMENTS

The authors gratefully acknowledge funding from the Gordon and Betty Moore Foundation through Grant No. 2645, the National Science Foundation Energy for Sustainability program (Grant No. CBET-0725164), and the Office of Naval Research through Grant No. N000141211047.

[1] S. Frandsen, "On the wind speed reduction in the center of large clusters of wind turbines," J. Wind Eng. Ind. Aerodyn. **39**, 251–265 (1992).
[2] J. Meyers and C. Meneveau, "Optimal turbine spacing in fully developed wind farm boundary layers," Wind Energy **15**, 305 (2011).
[3] B. Newman, "The spacing of wind turbines in large arrays," J. Energy Convers. **16**, 169–171 (1977).
[4] M. Z. Jacobson, *Fundamentals of Atmospheric Modeling* (Cambridge University Press, 2005).
[5] M. Méchali, R. Barthelmie, S. Frandsen, L. Jensen, and P. E. Réthoré, "Wake effects at Horns Rev and their influence on energy production," in *Proceedings of the 2006 European Wind Energy Association Conference in Athens, Greece* (Curran Associates, 2006), pp. 570–580, ISBN: 9781622764679.
[6] X. Yang, S. Kang, and F. Sotiropoulosa, "Computational study and modeling of turbine spacing effects in infinite aligned wind farms," Phys. Fluids **24**, 115107 (2012).
[7] R. B. Cal, J. Lebrón, L. Castillo, H. S. Kang, and C. Meneveau, "Experimental study of the horizontally averaged flow structure in a model wind-turbine array boundary layer," Renewable Sustainable Energy **2**, 013106 (2010).
[8] M. Calaf, C. Meneveau, and J. Meyers, "Large eddy simulation study of fully developed wind-turbine array boundary layers," Phys. Fluids **22**, 015110 (2010).
[9] L. P. Chamorro, R. E. A. Arndt, and F. Sotiropoulos, "Turbulent flow properties around a staggered wind farm," Boundary Layer Meteorol. **141**, 349–367 (2011).
[10] C. VerHulst and C. Meneveau, "Large eddy simulation study of the kinetic energy entrainment by energetic turbulent flow structures in large wind farms," Phys. Fluids **26**, 025113 (2014).
[11] M. Toloui, S. Riley, J. Hong, K. Howard, L. P. Chamorro, M. Guala, and J. Tucker, "Measurement of atmospheric boundary layer based on super-large-scale particle image velocimetry using natural snowfall," Exp. Fluids **55**, 1737 (2014).
[12] M. Kinzel, Q. Mulligan, and J. O. Dabiri, "Energy exchange in an array of vertical-axis wind turbines," J. Turbul. **13**, 1–13 (2012).
[13] E. Hau, *Wind Turbines* (Springer Verlag, Berlin, Heidelberg, 2006).
[14] R. J. Barthelmie, S. C. Pryor, S. T. Frandsen, K. S. Hansen, J. G. Schepers, K. Rados, W. Schlez, A. Neubert, L. E. Jensen, and S. Neckelmann, "Quantifying the impact of wind turbine wakes on power output at offshore wind farms," J. Atmos. Oceanic Technol. **27**, 1302–1317 (2010).
[15] K. Johnson and N. Thomas, "Wind farm control: Addressing the aerodynamic interaction among wind turbines," in *Proceedings of the 2009 American Control Conference in St. Louis, MO* (IEEE, 2009), pp. 2104–2109.
[16] D. Madjidian, K. Martensson, and A. Rantzer, "A distributed power coordination scheme for fatigue load reduction in wind farms," in *Proceedings of the 2011 American Control Conference in San Francisco, CA* (IEEE, 2011), pp. 5219–5224.
[17] J. Aho, A. Buckspan, J. Laks, P. Fleming, Y. Jeong, F. Dunne, M. Churchfield, L. Pao, and K. Johnson, "A tutorial of wind turbine control for supporting grid frequency through active power control," in *Proceedings of the 2012 American Control Conference in Montreal, QC* (IEEE, 2012), pp. 3120–3131.
[18] R. W. Whittlesey, S. Liska, and J. O. Dabiri, "Fish schooling as a basis for vertical axis wind turbine farm design," Bioinspiration Biomimetics **5**, 035005 (2010).
[19] J. O. Dabiri, "Potential order-of-magnitude enhancement of wind farm power density via counter-rotating vertical-axis wind turbine arrays," J. Renewable Sustainable Energy **3**, 043104 (2011).
[20] W. Zhu, R. van Hout, and J. Katz, "PIV measurements in the atmospheric boundary layer within and above a Mature Corn Canopy. Part II: Quadrant-hole analysis," J. Atmos. Sci. **64**, 2825–2838 (2006).
[21] G. Katul, D. Poggi, D. Cava, and J. Finnigan, "The relative importance of ejections and sweeps to momentum transfer in the atmospheric boundary layer," Boundary Layer Meteorol. **102**, 367–375 (2006).
[22] S. E. Belcher, N. Jerram, and J. C. R. Hunt, "Adjustment of a turbulent boundary layer to a canopy of roughness elements," J. Fluid Mech. **488**, 369–398 (2003).
[23] S. Lu and W. W. Willmarth, "Measurements of the structure of the Reynolds stress in a turbulent boundary layer," J. Fluid Mech. **60**, 481–511 (1973).
[24] W. Yue, C. Meneveau, M. B. Parlange, W. Zhu, R. van Hout, and J. Katz, "A comparative quadrant analysis of turbulence in a plant canopy," Water Resour. Res. **43**, W05422, doi:10.1029/2006WR005583 (2007).